remote sensing

MDPI

Technical Note

High-Efficiency Optimization Algorithm of PMEPR for OFDM Integrated Radar and Communication Waveform Based on Conjugate Gradient

Juan Rong [1,2], Feifeng Liu [2,3,*] and Yingjie Miao [2,3]

[1] School of Mathematics and Statistics, Beijing Institute of Technology, Beijing 100081, China; 3120170669@bit.edu.cn
[2] Key Laboratory of Electronic and Information Technology in Satellite Navigation, Ministry of Education, Beijing 100081, China; 3120170415@bit.edu.cn
[3] School of Information and Electronics, Beijing Institute of Technology, Beijing 100081, China
* Correspondence: feifengliu_bit@bit.edu.cn

Abstract: The tone reservation (TR) approach is mainly adopted to reduce the peak-to-mean envelope power ratio (PMEPR) of orthogonal frequency division multiplexing (OFDM) waveform with low TR ratio (TRR) in classic 4G communication systems. However, for the OFDM integrated radar and communication waveform, high TRR is necessary to simultaneously maintain the radar detection performance as well as communication performance. For cases with high TRR, the traditional waveform optimization algorithms have low execution efficiency and a poor PMEPR convergence level, and thus a new algorithm is needed. This paper proposes a new PMEPR optimization algorithm based on conjugate gradient. Firstly, by introducing the concept of L_p-norm, the PMEPR of the OFDM waveform is accurately remodeled as the objective function of the waveform optimization problem. Secondly, the conjugate gradient of the objective function is analytically derived to form the basis of the efficient PMEPR optimization. Finally, a PMEPR optimization algorithm based on the Polak–Ribière–Polyak (PRP) conjugate gradient is proposed. The simulation results verified the proposed algorithm in terms of optimization efficiency, as well as convergence level, and the initial experimental results suggested the practicality of the proposed algorithm.

Keywords: integrated radar and communications; orthogonal frequency division multiplexing; peak-to-mean envelope power ratio; conjugate gradient

Citation: Rong, J.; Liu, F.; Miao, Y. High-Efficiency Optimization Algorithm of PMEPR for OFDM Integrated Radar and Communication Waveform Based on Conjugate Gradient. *Remote Sens.* **2022**, *14*, 1715. https://doi.org/10.3390/rs14071715

Academic Editor: Gerardo Di Martino

Received: 10 February 2022
Accepted: 31 March 2022
Published: 2 April 2022

1. Introduction

Radar sensing and wireless communication are the two most common and important applications in modern radio technology. They are designed and developed independently according to different functions and frequency bands. Among them, radar is mainly used for target detection and identification, and the purpose of communication is to realize information transmission between devices. With the increasing requirements for high-quality communications and radar detection capabilities, the demand for radio frequency bandwidth is increasing, which makes the limited spectrum resources overcrowded. The integration of radar and communications is an effective way to solve the above problem [1–6].

The main challenge for the development of the integrated radar and communications is to find a waveform that can be used for both radar detection and communication information transmission. This is also a hot issue in the research of the integrated radar and communications. The researchers designed a variety of integrated radar and communication waveforms that fall into two main categories: multiplexing-waveform [7–11] and identical-waveform. The identity-waveform includes the radar-based waveform, which is a modified radar waveform with embedded communications information [12–16], and the communications-based waveform, which is the traditional communications waveform,

or their modified versions [17–21], the most famous being the orthogonal frequency division multiplexing (OFDM) integrated waveform.

As a multi-carrier modulation waveform, OFDM is widely used in radar, communications, and the integrated radar and communications. Compared with single-carrier waveforms, OFDM has many advantages, such as the availability of processing gains at the receiver, efficient spectrum utilization and good anti-multipath performance. However, due to the multi-carrier characteristics of OFDM, the superposition of subcarriers with the same phase usually results in a high peak-to-mean envelope power ratio (PMEPR). The high PMEPR problem is one of the most detrimental aspects in an OFDM integrated radar and communication system, as it degrades the efficiency of the power amplifier (PA) and causes nonlinear distortion [22], resulting in the degradation of radar and communication performance. Therefore, it is necessary to reduce PMEPR.

In order to reduce PMEPR, many methods have been proposed. Specifically, refs. [23,24] studied the method of generating a low PMEPR waveform by modulating the amplitude-phase. Although a closed form expression is given and is easy to apply, the obtained PMEPR is much higher than the optimal value, and the fixed modulation method limits the flexibility of these waveforms. Many techniques to reduce PMEPR have been proposed in communications [25–28]. The simplest technique is the limiting filter technique, which causes in-band distortion and deteriorates BER performance. Selective mapping (SLM) and partial transmission sequence (PTS) are known technologies, which may require that side information be transmitted as well. If the side information is received incorrectly at the receiver, the BER performance degrades. Tone reservation (TR) technology is proposed by Tellado [29], in which a small number of unused subcarriers are reserved to generate peak-canceling signal, and the rest are used to carry arbitrary information. Here, the ratio of the reserved subcarriers to the total number of subcarriers is defined as the TR ratio (TRR). TR does not need to transmit side information to the receiver, nor will BER decrease. The goal of TR is to find the reserved subcarriers that minimize PMEPR, which is expressed as the PMEPR optimization problem. This problem can also be formulated as a quadratically constrained quadratic program (QCQP) problem. Although the optimum QCQP problem exists, it requires high computational complexity. Sub-optimal solutions are typically employed. Specifically, ref. [30] proposed scaling the filtered limiting noise (i.e., generated by clipping the OFDM signal to a predetermined threshold) generated in the first iteration under TR constraints to generate peak-canceling signal. In addition, refs. [31–33] proposed a search method to solve the sub-optimal solutions. In [34], the peak of the signal was expressed in L_p-norm, and the PMEPR optimization technique was proposed based on the L_p-norm gradient.

The above TR methods are all proposed under low TRR, where the average power of the peak-canceling signal is excluded from the calculation of the average power in PMEPR. Since PMEPR is affected by the peak and valley of the waveform at the same time, ref. [19] introduced the coefficient of variation of envelopes as the objective function for waveform optimization, and developed an iterative least squares algorithm. However, this method is only applicable for a small number of subcarriers.

High resolution capability and long detection range are the goals of radar systems. Resolution is closely related to waveform bandwidth. With the increasing resolution of radar, the demand for waveform bandwidth is also increasing. This means that we reserve more subcarriers to obtain a lower PMEPR to achieve a longer radar detection range while maintaining a desired communication data rate. However, the high TRR implies that the average power of the peak-canceling signal in the PMEPR optimization problem is non-negligible, which means that the PMEPR reduction effect of the traditional TR method may be poor. Therefore, for the PMEPR optimization problem under high TRR, this paper transforms the PMEPR representation, which is difficult to directly optimize, into the ratio of the L_p-norm (with a large p) of the instantaneous power to the average power as the optimization objective function. We then propose an efficient and fast algorithm based on the classic Polak–Ribière–Polyak (PRP) conjugate gradient algorithm (PRP-CGA), which

is denoted as PRP-CG-based PMEPR optimization algorithm (PRP-CGPOA). In addition, some initial experiments are carried out to demonstrate the practicability of the proposed algorithm in terms of radar SNR and communication BER performance.

The rest of this paper is organized as follows. In Section 2, we briefly introduce the OFDM signal model, review the traditional PMEPR optimization problem and transform it into a new optimization problem based on L_p-norm with a large p. In Section 3, we give the gradient analytical model of the objective function and discuss the proposed PRP-CGPOA. Simulation and experimental demonstration results are given in Section 4. Finally, Section 5 summarizes the conclusions.

2. Integrated Signal Model

Consider a complex-valued OFDM waveform with N orthogonal subcarriers, where N_r subcarriers are reserved for a PMEPR reduction, and the others are used for data transmission. TRR is defined as $R = N_r/N$ $(1 \leq N_r < N)$. Let $\mathcal{R} = \{i_0, i_1, \ldots, i_{N_r-1}\}$ represent the index set of the reserved subcarriers, and $\mathcal{R}^c$ denote its complementary set in $\{-N/2, \ldots, N/2-1\}$. Therefore, the discrete-time OFDM waveform, after J times oversampling, is computed via an inverse discrete Fourier transform (IDFT) as

$$s(n) = \sum_{k=-N/2}^{N/2-1} (X_k + C_k) e^{j2\pi \frac{n}{JN} k} \tag{1}$$

where $n = 0, 1, \ldots, JN-1$. $X_k, k \in \mathcal{R}^c$ and $C_k, k \in \mathcal{R}$ represent the k-th modulated complex symbol in the information symbols $\mathbf{X}$ and the reserved symbols $\mathbf{C}$, respectively, and $X_k = 0$ for $k \in \mathcal{R}$ and $C_k = 0$ for $k \in \mathcal{R}^c$.

Denote $\mathbf{s} = [s(0), \ldots, s(JN-1)]^T \in \mathbb{C}^{JN\times 1}$. Then, (1) can be expressed in matrix form, i.e.,

$$\mathbf{s} = \mathbf{s}_c + \mathbf{F}_R \mathbf{C} \tag{2}$$

where $\mathbf{s}_c = \mathbf{F}_I \mathbf{X}$ represents the initial transmit waveform, $\mathbf{F}_I$ and $\mathbf{F}_R$ denote columns of the IDFT matrix $\mathbf{F} = \left(F_n^k\right)_{JN\times N} = \left(e^{j2\pi \frac{n}{JN} k}\right)_{JN\times N}$ indexed in $\mathcal{R}^c$ and $\mathcal{R}$, respectively.

The PMEPR of $\mathbf{s}$ is defined as the ratio of the maximal instantaneous power to the average power

$$\mathrm{PMEPR}_{s(n)} = \frac{\max\limits_{0\leq n\leq JN-1} |s(n)|^2}{E\left[|s(n)|^2\right]} \tag{3}$$

where $E\left[|s(n)|^2\right] = P_c + \sum\limits_{k\in\mathcal{R}} |C_k|^2$ is the average power, P_c is the total energy of $\mathbf{X}$. Actually, when $J \geq 4$, (3) is accurate enough to approximate the continuous-time counterpart [25].

For the traditional PMEPR optimization problem, TRR is typically low, with a value of 5–15% [35]. Then, $E\left[|s(n)|^2\right] \approx P_c$. The calculation for PMEPR can be simplified as

$$\mathrm{PMEPR}_{\mathbf{C}} = \frac{\max\limits_{0\leq n\leq JN-1} |s(n,\mathbf{C})|^2}{P_c} \tag{4}$$

here, $s(n) \triangleq s(n,\mathbf{C}) = s_c(n) + \mathbf{F}_{R,n}\mathbf{C}$, where $\mathbf{F}_{R,n}$ is the n-th row of $\mathbf{F}_R$. Thus, $\mathbf{C}$ must be chosen to minimize the maximum of the time-domain waveform, i.e.,

$$\mathbf{C}^{(\mathrm{opt})} = \arg\min_{\mathbf{C}} \max_{0\leq n\leq JN-1} |s(n,\mathbf{C})| \tag{5}$$

Then, (5) can be formulated as a QCQP [29], i.e.,

$$\begin{aligned} &\min_{\mathbf{C}} \xi \\ &s.t. \quad |s(n,\mathbf{C})| \leq \xi, \quad n = 0, 1, \ldots, JN-1 \end{aligned} \tag{6}$$

The communication community has developed different approaches to solve the problem in (6), such as [29–35].

Deformation of the Optimization Problem

In this paper, we focus on the PMEPR optimization problem of OFDM integrated radar and communication waveform, i.e.,

$$\min_{\mathbf{C}} \text{PMEPR}_{\mathbf{C}} = \frac{\max\limits_{0 \le n \le JN-1} |s(n, \mathbf{C})|^2}{P_c + \sum\limits_{k \in \mathcal{R}} |C_k|^2} \tag{7}$$

For the large-bandwidth OFDM integrated waveforms, TRR needs to be high, which can further reduce PMEPR to maintain a good communication performance while improving the radar detection range. However, the high TRR makes the denominator in problem (7) irreducible, i.e., the energy of $\mathbf{C}$ cannot be ignored.

The complementary cumulative distribution function (CCDF) is usually used to measure performance of PMEPR reduction, which gives the probability that the PMEPR exceeds a given threshold ζ and is defined as

$$\text{CCDF} = \Pr(\text{PMEPR} > \zeta) \tag{8}$$

The PMEPR performance of existing algorithms may be poor under the high TRR. For example, as shown in Figure 1. When $R = 50\%$, PMEPR reaches 8 dB at 10^{-4} probability, which is only 4.4 dB lower than the initial OFDM. Such a high PMEPR will seriously reduce the efficiency of the PA and affect the performance of the radar detection.

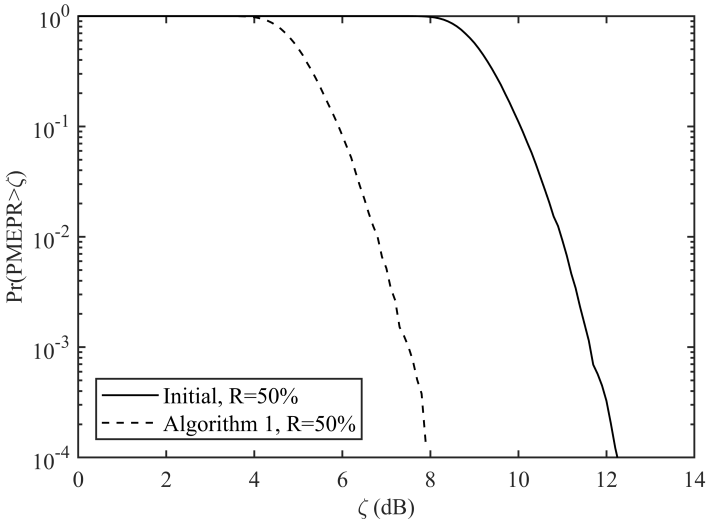

Figure 1. CCDFs of PMEPRs for random informative symbols, where Algorithm 1 is from [19].

Due to the denominator of the objective function, (7) is difficult to solve directly. The following uses the L_p-norm to transform (7) into an easy-to-solve form.

In mathematics, for a given vector $\mathbf{s}$, the L_p-norm is defined as

$$\|\mathbf{s}\|_p = \left(\sum_{n=0}^{JN-1} |s(n)|^p \right)^{1/p}, \quad \forall p \ge 1, p \in \mathbb{R} \tag{9}$$

Since L_p-norm is monotonically decreasing versus p, and $\|\mathbf{s}\|_\infty = \max_{0\le n\le JN-1} |s(n)| = \lim_{p\to\infty} \|\mathbf{s}\|_p$, we use the L_p-norm with a large p to approximate L_∞-norm. Then, (7) can be transformed into

$$\min_{\mathbf{C}} O(\mathbf{C}) = \frac{\left(\sum_{n=0}^{JN-1} |s(n,\mathbf{C})|^{2p}\right)^{1/p}}{P_c + \sum_{k\in\mathcal{R}} |C_k|^2} \tag{10}$$

According to $\left\||\mathbf{s}|^2\right\|_\infty < \left\||\mathbf{s}|^2\right\|_p$, $p < \infty$, we know that $\mathrm{PMEPR}_{\mathbf{C}} < O(\mathbf{C})$. Therefore, the sub-optimal solution of PMEPR can be obtained by solving problem (10). It can be seen from (10) that the objective function is an analytical expression about $\mathbf{C}$, which can be used for gradient analysis.

3. PRP-CGPOA

In this section, to guarantee that the objective function decreases monotonically and efficiently in each iteration, we adopt the classic PRP-CGA [36,37] to minimize the unconstrained problem (10), and propose the PRP-CGPOA. The flow chart of it is shown in Figure 2a. The conjugate gradient of $\mathbf{C}$ and the step size are the keys of PRP-CGPOA. In the following, we first derive them, and then summarize the whole algorithm.

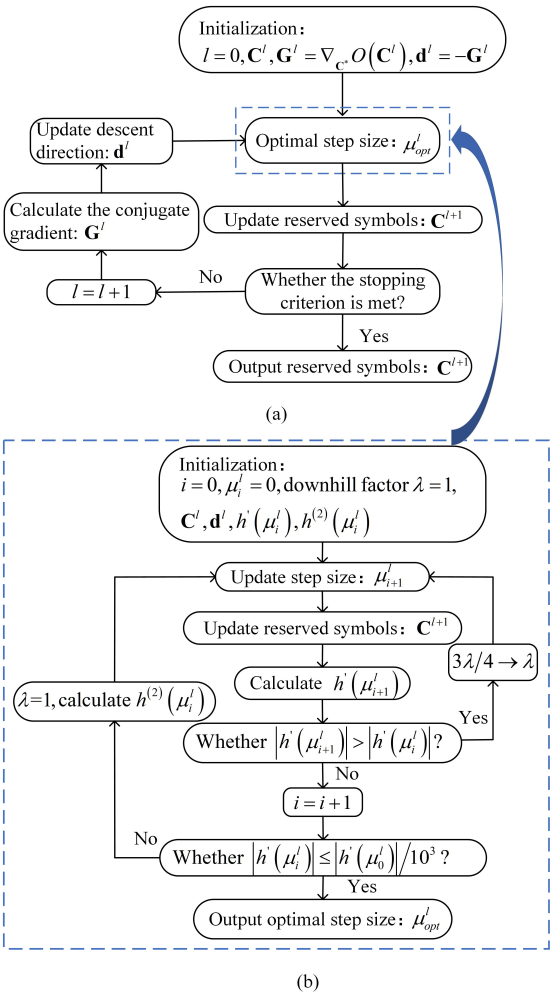

Figure 2. Flow chart of the overall algorithm and the step size optimization, (**a**) overall algorithm. (**b**) step size optimization.

3.1. Gradient Analytical Model

The analytic expression of the conjugate gradient in (10) with respect to $\mathbf{C}$ is given below. To facilitate the derivation, let $f(\mathbf{C}) = \left(\sum_{n=0}^{JN-1} |s(n,\mathbf{C})|^{2p} \right)^{1/p}$, $g(\mathbf{C}) = P_c + \sum_{k\in\mathcal{R}} |C_k|^2$. Then, the objective function $O(\mathbf{C})$ is written as $O(\mathbf{C}) = f(\mathbf{C})/g(\mathbf{C})$. Before deducing the conjugate gradient $\nabla_{\mathbf{C}^*} O(\mathbf{C})$, we calculate the derivative of $O(\mathbf{C})$ with respect to C_m^*, $m \in \mathcal{R}$, which is the conjugation of C_m. According to the derivation rule,

$$\frac{\partial O(\mathbf{C})}{\partial C_m^*} = \frac{\frac{\partial f(\mathbf{C})}{\partial C_m^*} g(\mathbf{C}) - f(\mathbf{C}) \frac{\partial g(\mathbf{C})}{\partial C_m^*}}{g^2(\mathbf{C})} \tag{11}$$

From (11), it is easy to see that $\partial f(\mathbf{C})/\partial C_m^*$ and $\partial g(\mathbf{C})/\partial C_m^*$ should be further simplified. Based on the expression of $f(\mathbf{C})$, $\partial f(\mathbf{C})/\partial C_m^*$ can be derived as follows

$$\begin{aligned} \frac{\partial f(\mathbf{C})}{\partial C_m^*} &= \frac{1}{p} \left(\sum_{n=0}^{JN-1} |s(n,\mathbf{C})|^{2p} \right)^{\frac{1-p}{p}} \sum_{n=0}^{JN-1} p|s(n,\mathbf{C})|^{2(p-1)} \frac{\partial |s(n,\mathbf{C})|^2}{\partial C_m^*} \\ &= (f(\mathbf{C}))^{1-p} \sum_{n=0}^{JN-1} |s(n,\mathbf{C})|^{2(p-1)} s(n,\mathbf{C}) \left(F_{R,n}^m\right)^* \\ &= (f(\mathbf{C}))^{1-p} (\mathbf{F}_R^m)^H \tilde{\mathbf{s}} \end{aligned} \tag{12}$$

where $\tilde{\mathbf{s}} = |\mathbf{s}|^{2(p-1)} \circ \mathbf{s}$, "$\circ$" is the Hadamard product, $\left(\mathbf{F}_R^m\right)^H$ represents the conjugate transpose of the m-th column of $\mathbf{F}_R$.

Based on the expression of $g(\mathbf{C})$, $\partial g(\mathbf{C})/\partial C_m^*$ can be derived as follows

$$\frac{\partial g(\mathbf{C})}{\partial C_m^*} = \frac{\partial \left(P_c + \sum_{k\in\mathcal{R}} |C_k|^2 \right)}{\partial C_m^*} = \frac{\partial (C_m C_m^*)}{\partial C_m^*} = C_m \tag{13}$$

By substituting (12) and (13) into (11), the derivative $\partial O(\mathbf{C})/\partial C_m^*$ is given by

$$\frac{\partial O(\mathbf{C})}{\partial C_m^*} = O(\mathbf{C}) \left((f(\mathbf{C}))^{-p} \left((\mathbf{F}_R^m)^H \tilde{\mathbf{s}} \right) - \frac{C_m}{g(\mathbf{C})} \right) \tag{14}$$

By stacking (14) into a vector, the conjugate gradient $\nabla_{\mathbf{C}^*} O(\mathbf{C})$ is obtained as follows

$$\nabla_{\mathbf{C}^*} O(\mathbf{C}) = \left[\frac{\partial O(\mathbf{C})}{\partial C_{-N/2}^*}, \ldots, \frac{\partial O(\mathbf{C})}{\partial C_{N/2-1}^*} \right]^T = O(\mathbf{C}) \left((f(\mathbf{C}))^{-p} \mathbf{F}_R^H \tilde{\mathbf{s}} - \frac{\mathbf{C}}{g(\mathbf{C})} \right) \tag{15}$$

3.2. Update Rules

The analytical expression (15) provides a strong support for our algorithm. The iterative update rule for $\mathbf{C}$ is as follows.

Assume that the l-th iteration point is $\mathbf{C}^l$, then the new iteration point $\mathbf{C}^{l+1}$ is

$$\mathbf{C}^{l+1} = \mathbf{C}^l + \mu^l \mathbf{d}^l \tag{16}$$

where μ^l is the step size.

The descent direction is another important part of the algorithm in addition to the conjugate gradient and the step size. In order to ensure that the algorithm is carried out efficiently, we adopt a modified descent direction, i.e., PRP descent direction, which is denoted as

$$\mathbf{d}^l = \begin{cases} -\mathbf{G}^l & l = 0 \\ -\mathbf{G}^l + \frac{(\mathbf{G}^l - \mathbf{G}^{l-1})^T \mathbf{G}^l}{\|\mathbf{G}^{l-1}\|^2} \mathbf{d}^{l-1} & l \geq 1 \end{cases} \tag{17}$$

where $\mathbf{G}^l = \nabla_{\mathbf{C}^*} O\left(\mathbf{C}^l\right)$.

3.3. Step Size

The calculation of the step size in each iteration is crucial to the convergence speed of the algorithm. The line search method is a classic method to obtain the step size. However, it needs to calculate the objective function many times, which makes it very time-consuming [37]. In this paper, we formulate the line search problem as a minimization problem of solving the step size, namely

$$\min_{\mu^l} h\left(\mu^l\right) = O\left(\mathbf{C}^{l+1}\right) = \frac{f\left(\mathbf{C}^{l+1}\right)}{g\left(\mathbf{C}^{l+1}\right)} \tag{18}$$

It can be seen from (18) that $h\left(\mu^l\right)$ is a complex high-order function of μ^l, which is difficult to calculate directly. However, similar to (11), the derivative of $h\left(\mu^l\right)$ with respect to μ^l can be derived, and so is the second derivative. Thus, we can solve the problem (18) using the classic Newton downhill method [38], the flow chart is shown in Figure 2b.

In the following, we derive the first and second derivatives of $h\left(\mu^l\right)$ with respect to μ^l.

The first derivative of $h\left(\mu^l\right)$ is

$$h'\left(\mu^l\right) = \frac{f'\left(\mathbf{C}^{l+1}\right)g\left(\mathbf{C}^{l+1}\right) - f\left(\mathbf{C}^{l+1}\right)g'\left(\mathbf{C}^{l+1}\right)}{g^2\left(\mathbf{C}^{l+1}\right)} \tag{19}$$

In order to get the expression of $h'\left(\mu^l\right)$, we first derive $f'\left(\mathbf{C}^{l+1}\right)$ and $g'\left(\mathbf{C}^{l+1}\right)$. From (16), we know that

$$s\left(n, \mathbf{C}^{l+1}\right) = s\left(n, \mathbf{C}^{l}\right) + \mu^l \mathbf{F}_{R,n}\mathbf{d}^l \tag{20}$$

Then, $f'\left(\mathbf{C}^{l+1}\right)$ and $g'\left(\mathbf{C}^{l+1}\right)$ can be expressed as

$$\begin{aligned} f'\left(\mathbf{C}^{l+1}\right) &= \left(f\left(\mathbf{C}^{l+1}\right)\right)^{1-p} \sum_{n=0}^{JN-1} |s\left(n, \mathbf{C}^{l+1}\right)|^{2(p-1)} \left(|s\left(n, \mathbf{C}^{l+1}\right)|^2\right)' \\ &= 2\left(f\left(\mathbf{C}^{l+1}\right)\right)^{1-p} \sum_{n=0}^{JN-1} |s(n, \mathbf{C}^{l+1})|^{2(p-1)} \mathrm{Re}\left(s(n, \mathbf{C}^{l+1})\left(\mathbf{F}_{R,n}\mathbf{d}^l\right)^*\right) \end{aligned} \tag{21}$$

$$g'\left(\mathbf{C}^{l+1}\right) = \left(P_c + \sum_{k\in\mathcal{R}} |C_k^{l+1}|^2\right)' = 2\sum_{k\in\mathcal{R}} \mathrm{Re}\left(C_k^{l+1}\left(d_k^l\right)^*\right) \tag{22}$$

For ease of presentation, let $\check{s}(n) = |s\left(n, \mathbf{C}^{l+1}\right)|^{2(p-1)}$, $\hat{s}(n) = \mathrm{Re}\left(s(n, \mathbf{C}^{l+1})\left(\mathbf{F}_{R,n}\mathbf{d}^l\right)^*\right)$, $\tilde{f} = \left(f\left(\mathbf{C}^{l+1}\right)\right)^{-p}$ and $A_d = \sum_{k\in\mathcal{R}} \mathrm{Re}\left(C_k^{l+1}\left(d_k^l\right)^*\right)$. Then, according to (19)–(22), $h'\left(\mu^l\right)$ can be rewritten as

$$h'\left(\mu^l\right) = 2O\left(\mathbf{C}^{l+1}\right)\left(\tilde{f}\sum_{n=0}^{JN-1}(\check{s}(n)\hat{s}(n)) - \frac{A_d}{g\left(\mathbf{C}^{l+1}\right)}\right) \tag{23}$$

According to (23), the second derivative of $h\left(\mu^l\right)$ is

$$h^{(2)}\left(\mu^l\right) = \frac{\left(h'\left(\mu^l\right)\right)^2}{O\left(\mathbf{C}^{l+1}\right)} + 2O\left(\mathbf{C}^{l+1}\right)\left[-2p\tilde{f}^2\left(\sum_{n=0}^{JN-1}\left(\check{s}(n)\hat{s}(n)\right)\right)^2 - \frac{d_{cons}}{g\left(\mathbf{C}^{l+1}\right)} + \frac{2A_d^2}{g^2\left(\mathbf{C}^{l+1}\right)}\right.$$
$$\left. + \tilde{f}\sum_{n=0}^{JN-1}\left(\check{s}(n)|\mathbf{F}_{R,n}\mathbf{d}^l|^2\right) + \tilde{f}\sum_{n=0}^{JN-1}\left(2(p-1)|s\left(n,\mathbf{C}^{l+1}\right)|^{(2(p-2))}\hat{s}^2(n)\right)\right] \tag{24}$$

where $d_{cons} = \sum_{k\in\mathcal{R}}|d_k^l|^2$.

After obtaining the expression of $h'\left(\mu^l\right)$ and $h^{(2)}\left(\mu^l\right)$, we can easily determine the search direction of μ^l, which is $-h'\left(\mu^l\right)/h^{(2)}\left(\mu^l\right)$. Then the update rule for μ^l is

$$\mu_{i+1}^l = \mu_i^l - \lambda\frac{h'\left(\mu_i^l\right)}{h^{(2)}\left(\mu_i^l\right)} \tag{25}$$

where i is the number of iterations, $\lambda \in (0,1]$ is the downhill factor, which needs to be dynamically adjusted during the iteration process to ensure that the objective function decreses stably.

The necessary condition for the objective function $h\left(\mu^l\right)$ to have an extremum is that the first derivative $h'\left(\mu^l\right) = 0$ at the extreme point. Therefore, in order to obtain the minimum point, the stopping criterion is set to be $|h'\left(\mu_i^l\right)| \le |h'\left(\mu_0^l\right)|/10^3$. According to Figure 2b, the optimal step size can be obtained.

3.4. Algorithm Summary and Complexity Comparison

Based on the above derivation, the new reserved symbol $\mathbf{C}^{l+1}$ is obtained in each iteration from Figure 2a. Then, according to (20), we have the new waveform $\mathbf{s}^{l+1}$, which is the optimum we want. In PRP-CGPOA, the stopping criterion can be set according to actual system requirements. For example, the PMEPR is not higher than a certain value, or the peak power of the integrated waveform is simply constrained.

We now quantify the computational complexity of our algorithm by the number of real multiplications and additions. Since the computational complexities of multiplication and addition operations are almost equivalent to those of division and subtraction, respectively, we refer here to divisions as multiplications and to subtractions as additions. A complex multiplication is counted as four real multiplications and two real additions and a complex addition requires two real additions. IFFT or FFT block requires $2JN\log_2(JN)$ real multiplications and $3JN\log_2(JN)$ real additions.

1. Complexity Analysis of PRP-CGPOA: each iteration is divided into three steps: (a) calculate the conjugate gradient $\nabla_{\mathbf{C}^*}O(\mathbf{C})$, (b) calculate the descent direction d^l, (c) calculate the step size μ^l. In steps (a) and (c), F_R^H/F_R related operations can be quickly implemented by FFT/IFFT. Here, the computational complexity of $(.)^{(1/p)}$ is regarded as a real multiplication and the computational complexity of the initialization stage in Figure 2a is omitted since it occurs only once.

In step (a), the computational complexity is $2JN\log_2(JN) + 4N_r + 2$ real multiplications and $3JN\log_2(JN) + 2N_r$ real additions.

In step (b), the computational complexity is $12N_r$ real multiplications and $8N_r$ real additions.

In step (c), it is assumed that the optimal step size is obtained by I iterations and the first derivative $h'(\mu^l)$ in Figure 2b is computed K times. Thus, the computational complexity of step (c) is $2JN\log_2(JN) + ((\log_2(p-2)+11)\mathrm{K} + 4\mathrm{I} + 13)JN + (6\mathrm{K}+4)N_r + 10\mathrm{K} + 8\mathrm{I} + 14$ real multiplications and $3JN\log_2(JN) + (8\mathrm{K}+2\mathrm{I}+7)JN + (5\mathrm{K}+3)N_r + 2\mathrm{K} + 4\mathrm{I} + 5$ real additions.

Therefore, the computational complexity of PRP-CGPOA is $4JN\log_2(JN) + ((\log_2(p-2)$ $+11)\mathrm{K} + 4\mathrm{I} + 13)JN + (6\mathrm{K}+20)N_r + 10\mathrm{K} + 8\mathrm{I} + 16$ real multiplications and $6JN\log_2(JN) +$ $(8\mathrm{K}+2\mathrm{I}+7)JN + (5\mathrm{K}+13)N_r + 2\mathrm{K} + 4\mathrm{I} + 5$ real additions.

2. Complexity Analysis of [19]: Assuming that the amplitude calculation for each sample in the integrated waveform is treated as a real multiplication, the complexity in each iteration is $2JN\log_2(JN) + 4N_rJN + 5JN + 1$ real multiplications and $3JN\log_2(JN) + 4N_rJN + 4JN + 2N_r$ real additions.

3. Complexity Analysis of the Classic Iterative Clipping and Filtering (ICF) Algorithm [28]: The complexity in each iteration is mainly determined by the JN-point FFT/IFFT pair, which is $4JN\log_2(JN) + 2JN$ real multiplications and $6JN\log_2(JN) + 2JN$ real additions.

For each iteration, the complexity difference between PRP-CGPOA and [28] is $O(JN)$, whereas they both differ from [19] mainly by $O(N_rJN)$, so the complexity of PRP-CGPOA is higher than that of [28], but lower than that of [19]. To evaluate computational complexity, the iteration numbers and runtime that achieve the same PMEPR reduction performance need to be discussed. In Section 4, we will compare the PMEPR performance of these algorithms.

4. Results

4.1. Simulation Analysis

In this section, we mainly simulate and verify the PMEPR optimization performance of the proposed algorithm. Here, the OFDM integrated radar and communication waveform we are discussing have multiple subcarriers, and continuous subcarriers are reserved near the center frequency, i.e., $\mathcal{R} = \{-(N_r/2), -(N_r/2)+1, \ldots, (N_r/2)-1\}$. The parameter settings are shown in Table 1. In this paper, $R = 50\%$ is mainly discussed, i.e., the entire bandwidth of the integrated waveform is used for radar detection, and half of the bandwidth is used to transmit communication information.

Table 1. Simulation parameters.

Parameter	Value
Pulse Width	10 μs
Bandwidth	100 MHz
Sampling Frequency	400 MHz
Number of Subcarriers	1000
Modulation	16 QAM
TRR	50%

To generate the CCDF of the PMEPR, 10^5 16-quadratic-amplitude-modulated (16QAM) initial OFDM symbols are randomly generated, where the reserved subcarriers are set to 0, i.e., $\mathbf{C}^0 = \mathbf{0}$. In the L_p-norm, $p = 26$.

Randomly select an OFDM symbol, and after PRP-CGPOA optimization, the final integrated waveform is obtained. Figure 3 shows the envelopes of the integrated waveform after 143 iterations and the initial waveform. It can be observed that the average power of the integrated waveform is significantly increased, which reduces the PMEPR from 8.7 dB to 2.3 dB. According to the radar equation [39], the integrated waveform with high average transmit power enables long-range detection.

The PMEPR and the objective function of (10) versus the number of iterations are calculated and shown in Figure 4, and the PMEPR obtained by [19,28] are also shown for comparative analysis. As shown in Figure 4, the objective function of (10) on the right axis is monotonically reduced, and the overall trend of PMEPR obtained by PRP-CGPOA on the left axis is decreasing, but not monotonically decreasing, unless p approaches infinity. Compared with [19,28], PRP-CGPOA can achieve high PMEPR reduction gain with less iterations.

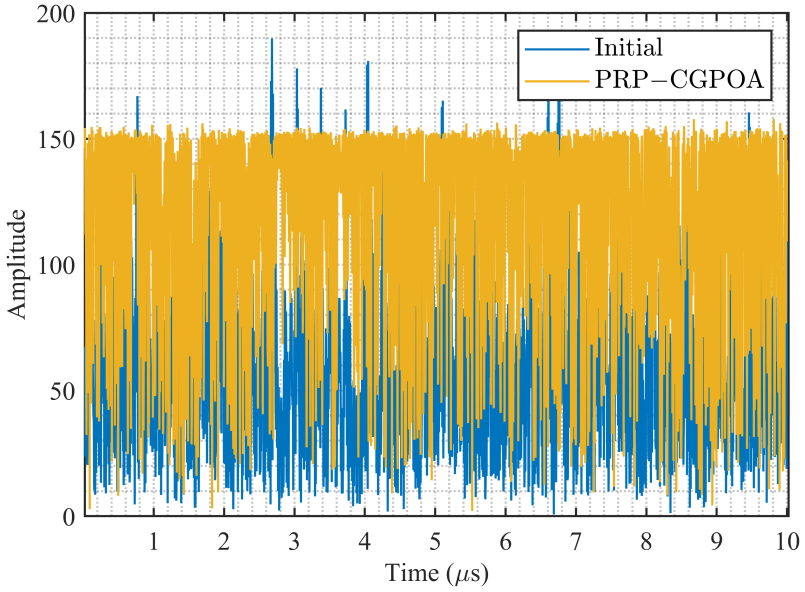

Figure 3. Envelopes of the initial and integrated waveform.

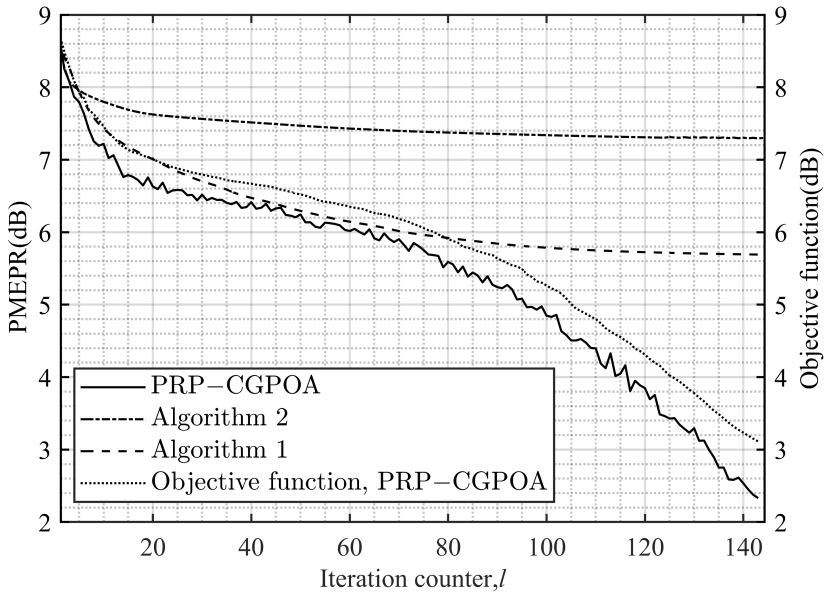

Figure 4. PMEPRs and objective function in (10) versus the iteration numbers, where Algorithm 1 is from [19] and Algorithm 2 is from [28].

Figure 5 shows some comparisons of these three PMEPR reduction algorithms with a PMEPR threshold of 3 dB. For CCDF = 10^{-4}, PRP-CGPOA obtains 9.4 dB PMEPR reduction, which is 5 dB better than [19] and 6.7 dB better than [28].

To analyze the computational complexity, Figure 6 plots the iteration numbers that achieve the same PMEPR as a function of the achieved PMEPR of the three algorithms. It can be observed that the number of iterations increases as the PMEPR decreases. For a desired PMEPR of less than 6 dB, PRP-CGPOA requires fewer iteration numbers than others, which shows that PRP-CGPOA has the lowest complexity. However, for a PMEPR greater than 6 dB, PRP-CGPOA requires more iteration numbers than [19], which does not mean higher complexity, because the complexity of a single iteration in PRP-CGPOA is lower than that of [19]. Therefore, it is necessary to compare the runtime of the achieved PMEPR. Specially, to achieve a 6 dB/7 dB PMEPR, the runtime of PRP-CGPOA and [19] are 19.2 ms/8.3 ms and 62.6 ms/17.9 ms, respectively. Since the 6 dB PMEPR obtained

by [28] may require a large number of iterations, only the 7 dB PMEPR is considered, and the runtime is 33.6 ms. Thus, compared with the other two algorithms, PRP-CGPOA has lower complexity to obtain the same PMEPR. Comparisons of these algorithms are further listed in Table 2. The PRP-CGPOA achieves a 5 dB improvement in PMEPR at 1/7 of the runtime of [19], and 6.7 dB improvement in PMEPR at 1/2.6 of the runtime of [28]. Therefore, the integrated waveform with high PMEPR reduction performance can be efficiently generated by PRP-CGPOA.

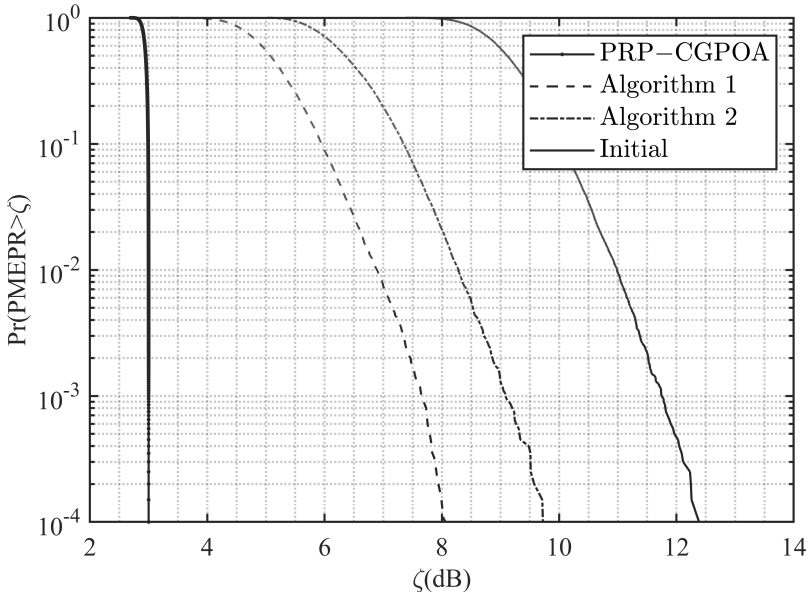

Figure 5. PMEPR reduction comparison for three algorithms, where Algorithm 1 is from [19] and Algorithm 2 is from [28].

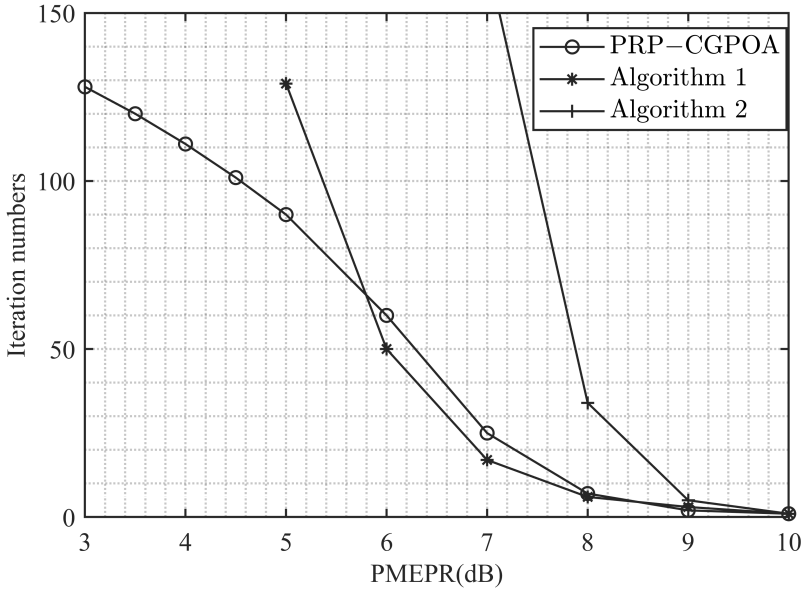

Figure 6. Iteration numbers in complexity analysis versus achieved PMEPR, where Algorithm 1 is from [19] and Algorithm 2 is from [28].

Table 2. PMEPR reduction and runtime comparison of PRP-CGPOA, Refs. [19,28] to achieve 3 dB PMEPR.

Algorithm	PRP-CGPOA	[19]	[28]
PMEPR reduction	9.4 dB	4.4 dB	2.7 dB
Runtime	41.9 ms	299.8 ms	110.4 ms

4.2. Experimental Demonstration

In this section, some initial experiments are conducted to demonstrate the practicality of the proposed algorithm. A total of 136 OFDM symbols before and after PMEPR optimization of the proposed algorithm are used as transmit waveforms for target detection and communication decoding, respectively, to analyze the influence of PMEPR optimization on radar SNR and communication BER performance. Figure 7 shows the PMEPR performance of the transmit waveforms optimized by the proposed algorithm, where the integrated waveform has a PMEPR gain of about 6.5 dB.

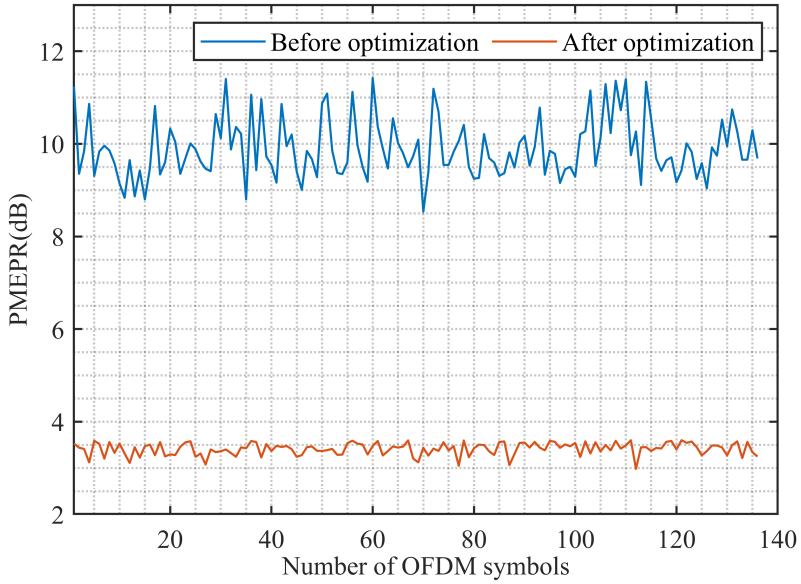

Figure 7. PMEPRs of different OFDM symbols before and after PMEPR optimization.

The integrated radar and communication system we adopted consists of two nodes, A and B, both of which contain two antennas. Node A is a transceiver for detection, and the two antennas of node B are both detected by node A as strong scatters, and receive direct waves from node A for communication decoding. The system parameters are: Pulse width of 100 μs, signal bandwidth of 100 MHz, sampling frequency of 125 MHz and carrier frequency of 1.5 GHz. The schematic diagram of the experiment is shown in Figure 8, where node A is about 60 m away from node B, and the two antennas of the same node are about 1.5 m apart. Figure 9 is the echo waveforms received by node A. Pulse compression is performed on the echoes. It can be seen from Figure 10 that there are two targets at 55.04 m and 57.24 m, respectively, corresponding to the two antennas of node B. Then, the echo SNR is analyzed, as shown in Figure 11. It can be observed that the average relative SNR after and before PMEPR optimization is about 6.2 dB, which means that the integrated waveform obtained by the proposed algorithm has better radar SNR performance. The communication data are decoded on the direct waves received by node B. Figure 12 is the echo constellation diagrams after channel equalization. From the comparison before and after PMEPR optimization, it can be seen that there is no significant change, and the BERs are 5.198×10^{-4} and 5.1976×10^{-4}, which are approximately the same.

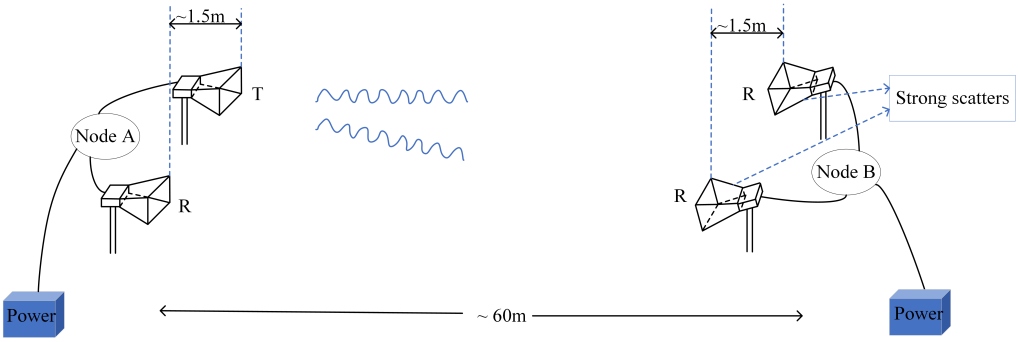

Figure 8. Schematic diagram of the experiment.

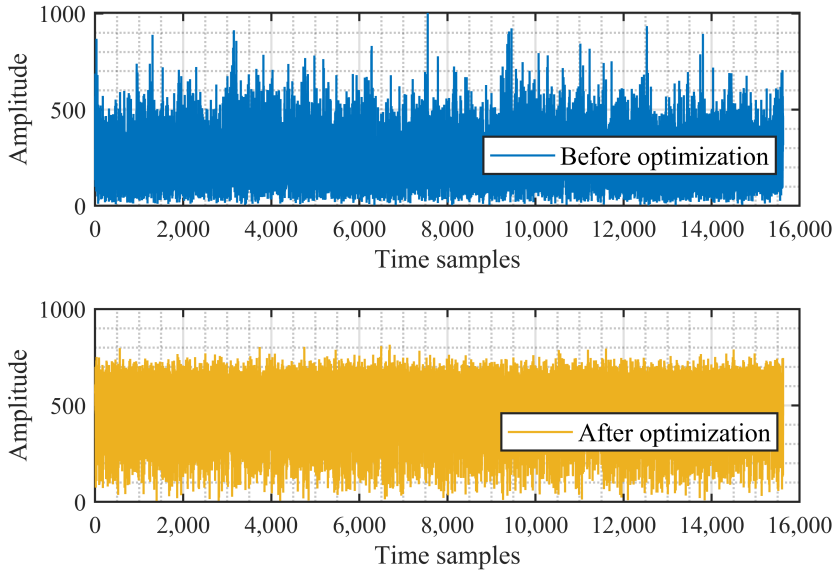

Figure 9. Echo waveform s for different OFDM symbols.

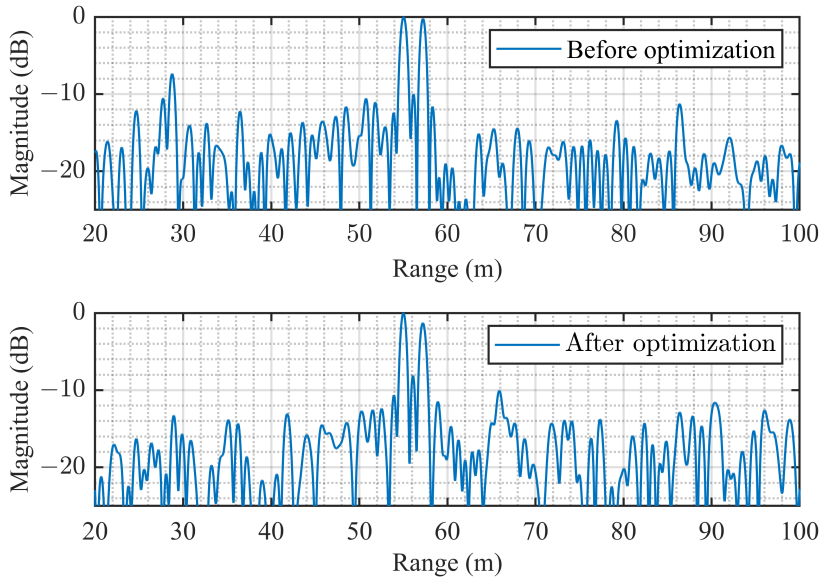

Figure 10. Range profiles.

It can be suggested from the initial experimental results that the proposed PMEPR optimization algorithm can significantly improve the radar SNR performance while maintaining the communication BER performance.

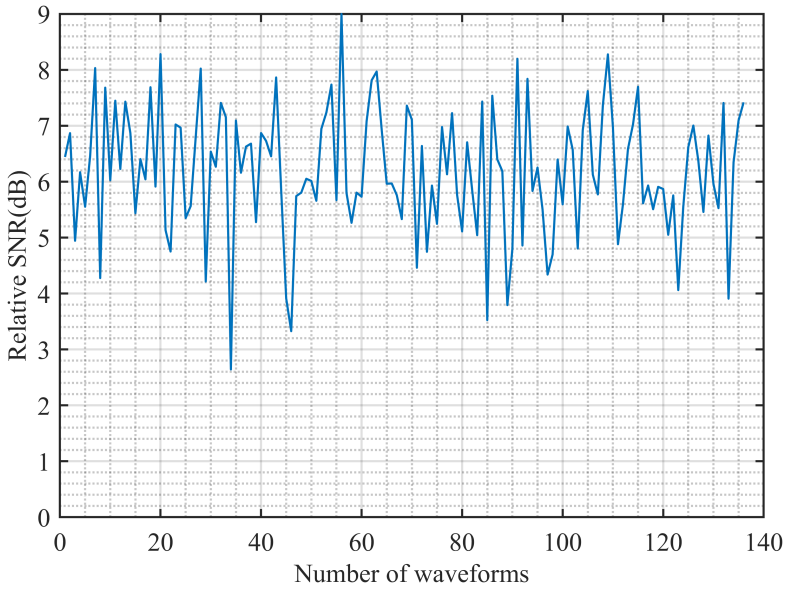

Figure 11. Relative SNR after and before PMEPR optimization.

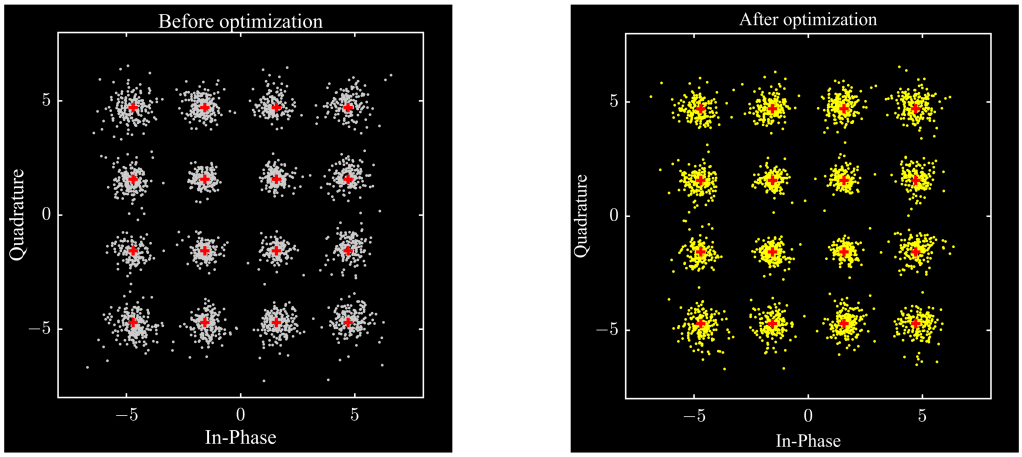

Figure 12. Echo constellation diagrams before and after PMEPR optimization. (**a**) Before. (**b**) After.

5. Conclusions

This paper dealt with the PMEPR optimization problem of the OFDM integrated waveform with high TRR. To cope with the difficult problem of directly optimizing PMEPR, the ratio of the L_p-norm of instantaneous power to the average power was firstly introduced to approximate PMEPR with very high accuracy in the paper. By establishing the gradient analytical model of the objective function, i.e., L_p-norm of PMEPR, the PRP-CGPOA that uses the PRP-CGA was introduced to solve the PMEPR optimization problem. The simulation results show that the proposed algorithm reduces PMEPR efficiently and quickly. The initial experiments are conducted and show that the proposed algorithm can significantly improve the radar SNR performance while maintaining the communication BER performance, which is practical. For a general radar system, PA usually works at saturation level, which is not the case for the classic communication system. Therefore, a trade-off between

radar performance and communication performance when the integrated waveform is used in the integrated system must be evaluated, which will be further studied in future work.

Author Contributions: Conceptualization, J.R.; validation, J.R. and F.L.; investigation, J.R.; writing—original draft preparation, J.R.; writing—review and editing, F.L. and Y.M.; supervision, F.L. All authors have read and agreed to the published version of the manuscript.

Funding: This research was supported by the Special Fund for Research on National Major Research Instruments (grant No. 31727901) and the National Natural Science Foundation of China (grant No. 62071045 and grant No. 61625103).

Institutional Review Board Statement: Not applicable.

Informed Consent Statement: Not applicable.

Data Availability Statement: The data that support the findings of this study are available from the corresponding author, F.L., upon reasonable request.

Conflicts of Interest: The authors declare no conflict of interest.

References

1. Chiriyath, A.R.; Paul, B.; Jacyna, G.M.; Bliss, D.W. Inner bounds on performance of radar and communications co-existence. *IEEE Trans. Signal Process.* **2016**, *64*, 464–474. [CrossRef]
2. Feng, Z.; Fang, Z.; Wei, Z.; Chen, X.; Quan, Z.; Li, D. Joint radar and communication: A survey. *China Commun.* **2020**, *17*, 1–27. [CrossRef]
3. Xiao, B.; Huo, K.; Liu, Y. Development and prospect of radar and communication integration. *J. Electron. Inf. Technol.* **2019**, *41*, 739–750.
4. Luong, N.C.; Lu, X.; Hoang, D.T.; Niyato, D.; Kim, D.I. Radio resource management in joint radar and communication: A comprehensive survey. *IEEE Commun. Surv. Tutor.* **2021**, *23*, 780–814. [CrossRef]
5. Hassanien, A.; Amin, M.G.; Zhang, Y.D.; Ahmad, F. Signaling strategies for dual-function radar communications: An overview. *IEEE Aerosp. Electron. Syst. Mag.* **2016**, *31*, 36–45. [CrossRef]
6. Sturm, C.; Wiesbeck, W. Waveform design and signal processing aspects for fusion of wireless communications and radar sensing. *Proc. IEEE* **2011**, *99*, 1236–1259. [CrossRef]
7. Han, L.; Wu, K. Multifunctional transceiver for future intelligent transportation systems. *IEEE Trans. Microw. Theory Tech.* **2011**, *59*, 1879–1892. [CrossRef]
8. Moghaddasi, J.; Wu, K. Multifunctional transceiver for future radar sensing and radio communicating data-fusion platform. *IEEE Access* **2016**, *4*, 818–838. [CrossRef]
9. Takase, H.; Shinriki, M. A dual-use radar and communication system with complete complementary codes. In Proceedings of the 2014 15th International Radar Symposium (IRS), Gdansk, Poland, 16–18 June 2014.
10. Romero, R.A.; Shepherd, K.D. Friendly spectrally shaped radar waveform with legacy communication systems for shared access and spectrum management. *IEEE Access* **2015**, *3*, 1541–1554. [CrossRef]
11. Shi, C.; Wang, F.; Salous, S.; Zhou, J. Joint subcarrier assignment and power allocation strategy for integrated radar and communications system based on power minimization. *IEEE Sens. J.* **2019**, *19*, 11167–11179. [CrossRef]
12. Hassanien, A.; Amin, M.G.; Zhang, Y.D.; Ahmad, F. Dual-function radar-communications: Information embedding using sidelobe control and waveform diversity. *IEEE Trans. Signal Process.* **2015**, *64*, 2168–2181. [CrossRef]
13. Gu, Y.; Zhang, L.; Zhou, Y.; Zhang, Q. Embedding communication symbols into radar waveform with orthogonal FM scheme. *IEEE Sens. J.* **2018**, *18*, 8709–8719. [CrossRef]
14. Chen, X.; Wang, X.; Xu, S.; Zhang, J. A novel radar waveform compatible with communication. In Proceedings of the 2011 International Conference on Computational Problem-Solving, Chengdu, China, 21–23 October 2011.
15. Sahin, C.; Jakabosky, J.; McCormick, P.M.; Metcalf, J.G.; Blunt, S.D. A novel approach for embedding communication symbols into physical radar waveforms. In Proceedings of the 2017 IEEE Radar Conference (RadarConf), Seattle, WA, USA, 8–12 May 2017.
16. Pappu, C.S.; Beal, A.N.; Flores, B.C. Chaos based frequency modulation for joint monostatic and bistatic radar-communication systems. *Remote Sens.* **2021**, *13*, 4113. [CrossRef]
17. Liu, Y.; Liao, G.; Xu, J.; Yang, Z.; Zhang, Y. Adaptive OFDM integrated radar and communications waveform design based on information theory. *IEEE Commun. Lett.* **2017**, *21*, 2174–2177. [CrossRef]
18. Cheng, S.; Wang, W.; Shao, H. Spread spectrum-coded OFDM chirp waveform diversity design. *IEEE Sens. J.* **2015**, *15*, 5694–5700. [CrossRef]
19. Huang, T.; Zhao, T. Low PMEPR OFDM radar waveform design using the iterative least squares algorithm. *IEEE Signal Process. Lett.* **2015**, *22*, 1975–1979. [CrossRef]
20. Wang, Z.; Su, Y.; Cui, Z.; Su, X. A design of communication radar integrated signal of MCPC based on costas coding. In Proceedings of the 2019 IEEE 4th International Conference on Image, Vision and Computing (ICIVC), Xiamen, China, 5–7 July 2019.

21. Ahmed, A.; Zhang, Y.D.; Hassanien, A. Joint radar-communications exploiting optimized OFDM waveforms. *Remote Sens.* **2021**, *13*, 4376. [CrossRef]
22. Nee, R.V.; Prasad, R. *OFDM for Wireless Multimedia Communications*; Artech House: Boston, MA, USA, 2000.
23. Levanon, N. *Radar Signals*; John Wiley & Sons, Inc.: Hoboken, NJ, USA, 2004.
24. Narahashi, S.; Nojima, T. New phasing scheme of n-multiple carriers for reducing peak-to-average power ratio. *Electron. Lett.* **1994**, *30*, 1382–1383. [CrossRef]
25. Rahmatallah, Y.; Mohan, S. Peak-to-average power ratio reduction in OFDM systems: A survey and taxonomy. *IEEE Commun. Surv. Tutor.* **2013**, *15*, 1567–1592. [CrossRef]
26. Jiang, T.; Wu, Y. An overview: Peak-to-average power ratio reduction techniques for OFDM signals. *IEEE Trans. Broadcast.* **2008**, *54*, 257–268. [CrossRef]
27. Han, S.H.; Lee, J.H. An overview of peak-to-average power ratio reduction techniques for multicarrier transmission. *IEEE Wirel. Commun.* **2005**, *12*, 56–65. [CrossRef]
28. Armstrong, J. Peak-to-average power reduction for OFDM by repeated clipping and frequency domain filtering. *Electron. Lett.* **2002**, *38*, 246–247. [CrossRef]
29. Tellado, J. Peak to Average Power Reduction for Multicarrier Modulation. Ph.D. Thesis, Stanford University, Stanford, CA, USA, 1999.
30. Wang, L.; Tellambura, C. Analysis of clipping noise and tonereservation algorithms for peak reduction in OFDM systems. *IEEE Trans. Veh. Technol.* **2008**, *57*, 1675–1694. [CrossRef]
31. Chen, J.C.; Chiu, M.H.; Yang, Y.S.; Li, C.P. A suboptimal tone reservation algorithm based on cross-entropy method for PAPR reduction in OFDM systems. *IEEE Trans. Broadcast.* **2011**, *57*, 752–756. [CrossRef]
32. Wang, Y.; Chen, W.; Tellambura, C. Genetic algorithm based nearly optimal peak reduction tone set selection for adaptive amplitude clipping PAPR reduction. *IEEE Trans. Broadcast.* **2012**, *58*, 462–471. [CrossRef]
33. Lim, D.W.; Noh, H.S.; No, J.S.; Shin, D.J. Near optimal PRT set selection algorithm for tone reservation in OFDM systems. *IEEE Trans. Broadcast.* **2008**, *54*, 454–460.
34. Janaaththanan, S.; Kasparis, C.; Evans, B.G. A gradient based algorithm for PAPR reduction of OFDM using tone reservation technique. In Proceedings of the VTC Spring 2008—IEEE Vehicular Technology Conference, Singapore, 11–14 May 2008.
35. Hou, J.; Ge, J.; Gong, F. Tone reservation technique based on peak-windowing residual noise for PAPR reduction in OFDM systems. *IEEE Trans. Veh. Technol.* **2015**, *64*, 5373–5378. [CrossRef]
36. Polak, E.; Ribière, G. Note sur la convergence de directions conjugèes. *Rev. Fr. Inform. Rech. Oper.* **1969**, *16*, 35–43.
37. Liang, T.; Zhu, Y.; Fu, Q. Designing PAR-constrained periodic/aperiodic sequence via the gradient-based method. *Signal Process.* **2018**, *147*, 11–22.
38. Zhang, X. *Matrix Analysis and Applications*; Tsinghua University Press: Beijing, China, 2004.
39. Ding, L.; Geng, F. *Principle of Radar*, 3rd ed.; Xidian University Press: Xi'an, China, 2002.